Structure and magnetism in bcc-based iron-cobalt alloys

A. Díaz-Ortiz,[1,2] R. Drautz,[3] M. Fähnle,[2] H. Dosch,[2] and J. M. Sanchez[1]
[1]*Texas Materials Institute, The University of Texas at Austin, 78712 Austin, TX, USA*
[2]*Max-Planck-Institut für Metallforschung, Heisenbergstraße 3, D-70569 Stuttgart, Germany*
[3]*Department of Materials, University of Oxford, Parks Road, Oxford OX1 3PH, United Kingdom*
(Received 29 March 2006; revised manuscript received 12 May 2006; published 29 June 2006)

The ordering and magnetic properties of bcc-based iron-cobalt alloys have been investigated as a function of the atomic composition. The different states of ordering in Fe-Co alloys, from the fully ordered to the disordered state, and their effect on the atomic volume, the magnetic moment, and enthalpy of formation, were described using the recently developed variational cluster expansion method based on first-principles data. The coarse-grained description of the energetics of the system allowed one to identify several new ordered structures, additional to the known FeCo-B2 (CsCl) ground state, after an extensive combinatorial search in the configurational phase space. It is found that the atomic volume and magnetic moment do not follow Vergard's law for either the ordered or disordered Fe-Co alloys. However, the equilibrium values of the atomic volume and the magnetic moment depend linearly on each other. The implications of such results on Fe-Co nanostructured systems are discussed.

DOI: 10.1103/PhysRevB.73.224208 PACS number(s): 61.66.Dk, 71.15.Nc, 75.20.En

I. INTRODUCTION

Alloys of iron and cobalt constitute an important class of soft magnetic materials with a wide and important range of technological applications where high magnetic flux densities are required. Fe-Co alloys find application in data storage, high performance transformers, and pole tips for high field magnets.[1] More recently, efforts in devising a new generation of aircrafts, where the pneumatic, hydraulic, and mechanical components are to be replaced by their electric and magnetic counterparts, have focused on developing new alloys that can meet the stringent operation conditions of an aircraft, i.e., alloys that can perform at high temperatures ($\sim$600 °C) while sustaining high inductions and good thermal stability for extended periods of time ($\sim$5000 h). The More Electric Aircraft initiative[2] has found Fe-Co based alloys the material of choice because of their unique combination of high saturation magnetization, high Curie temperatures, good permeability, good strengths, and excellent performance-to-weight ratio.[1,2]

Scientifically, on the other hand, iron-cobalt alloys pose interesting questions because of their structural and physical properties.[3] At high temperatures the fcc-based Fe-Co alloys are stable (austenite), transforming into bcc-based (ferrite) structures upon lowering the temperature. Fe-Co alloys are ferromagnetic in the whole composition range with Curie temperatures that decrease linearly with composition for Co-rich alloys, while coinciding with the austenite-to-ferrite transition temperature ($T\sim$985 °C) for near stoichiometric FeCo alloys. At lower temperatures, the system undergoes an order-disorder transformation between the bcc disordered (α) phase and the B2 (CsCl-type, α') phase. The ordered B2 phase exists over a considerable concentration range around equiatomic composition, i.e., between 28 and 75 at. % Fe with a maximum order-disorder temperature of $\sim$730 °C. The assessed temperature-concentration phase diagram of Nishizawa and Ishida shows no other stable intermetallic phases for temperatures higher than 500 °C.[4] However, over the years it has been suggested that additional intermetallic phases are present at lower temperatures.[5–7] Masumoto *et al.*[5] proposed the existence of $FeCo_3$ and Fe_3Co superstructures based on their heat-capacity and electric conductivity measurements, where maxima for such quantities were found around the 25 and 75 at. % Fe. Subsequently, Viting[6] and Goldenberg *et al.*[7] also found, by different methods, signs of both superlattices. There are also investigations that do not support the existence of other ordered structures additional to the FeCo-B2 phase. Asano and co-workers,[8] based upon their neutron diffraction and Mössbauer measurements on Fe-Co fine particles, ruled out the existence of the Fe_3Co structure. However, recent nuclear-magnetic resonance experiments by Wojcik and co-workers[9] on codeposited Fe-Co thin films seem to verify the early claims of new Fe-Co ordered structures. Very recently, on the basis of first-principles electronic structure calculations and combinatorial analysis, we found that Fe-Co alloys display a dense sequence of ground states additional to the known B2 phase.[10] Our results showed that the $L6_0$ phase (Ti_3Cu-type) is stable against phase separation between neighboring phases, i.e., between the $Fe_{11}Co_5$ and the $Fe_{13}Co_3$, thus constituting a true Fe_3Co ground-state structure.

This paper aims to provide an integral picture of the interplay between structure and magnetism in bcc-based Fe-Co alloys by enlarging the analysis of the energetics of Fe-Co at low temperatures advanced in Ref. 10, and by expanding it to other physical quantities of interest, such as the atomic volume and the magnetic moment. Particular emphasis has been set on the different degrees of partial order and their impact on the aforementioned quantities when the atomic concentration is varied. The formalism of the cluster expansion[11,12] is used to bridge the quantum-mechanical description of several ordered structures with the statistical mechanics necessary to model partially ordered alloys. This allows us to make the proper comparisons with experimental[3] and previous theoretical work,[13–18] especially with those within the virtual crystal[19,20] or the coherent-potential approximation,[21–25] that aimed to describe the magnetic

properties of disordered Fe-Co alloys. Our theoretical results show good agreement with the available experimental data.

The theoretical tools are discussed in Sec. II, where the recently developed variational approach to the cluster expansion[27] is presented in detail, together with the mixed-basis plane-wave pseudopotential technique employed to generated the first-principles Fe-Co data. The results are presented in Sec. III followed by discussions on the existence of the Fe_3Co superlattices and on the implications of a dense sequence of ground-state structures for nanostructured iron-cobalt alloys. The paper is closed with a summary of the results and the conclusions.

II. THEORY

A. Cluster expansion method

The cluster expansion method[11,12] is commonly applied in crystals where each atom can be assigned to a lattice site p. For binary systems, the occupation variable $\sigma_p=+1(-1)$ when lattice site p is occupied by the atomic species $A(B)$, respectively. The whole crystal with N lattice sites is characterized by the configuration vector of the occupation of all lattice sites $\boldsymbol{\sigma}_i=\{\sigma_1,\sigma_2,\ldots,\sigma_N\}$. The cluster expansion method states that *any function* F of the alloy configuration can be expressed as[11,12]

$$F(\boldsymbol{\sigma}_i)=J_0+\sum_{\alpha} D_\alpha J_\alpha \Phi_\alpha(\boldsymbol{\sigma}_i), \tag{1}$$

where $\Phi_\alpha(\boldsymbol{\sigma}_i)$ are the lattice averages of the cluster functions, defined as the product of the occupation variables on the cluster of α lattice points, J_α are the effective cluster interactions (ECIs), and the D_α account for the number of symmetry-equivalent clusters having identical effective cluster interactions. Examples of alloy functions that depend on the configuration are the atomic volume, the magnetic moment and, of course, the enthalpy of formation.

An important characteristic of Eq. (1) is that the Φ_α constitute a complete set of basis functions in the configuration space.[11] In other words, once the corresponding expansion coefficients J_α are determined, we can easily compute F for *any configuration* $\boldsymbol{\sigma}$ of the system, including all ordered and disordered states. Rigorously, the determination of an infinite number of ECIs needs an infinite set of configurations. The viability of Eq. (1) resides in the notion that configurational degrees of freedom and the crystal structures in metals are strongly correlated and thus amenable to be described by a small number of parameters.[28] In the past two decades, a wealth of work on alloys and surfaces thereof, have been done using the cluster expansion thus establishing it as a reliable tool for describing *ab initio* configurational thermodynamics of alloys.[29,30]

The practical implementation of Eq. (1) relies on the knowledge of F for a given set of ordered structures, i.e., for a certain set of $\boldsymbol{\sigma}$'s, so that the expansion can be inverted, that is, the expansion coefficients (ECIs) can be determined. This is easily accomplished by truncating the expansion and retaining a small number of terms (10–20). Deciding which terms ought to be included is a different matter and has been the subject of protracted discussions in the literature.[29–33] Historically, due to the technical difficulties to large and reliable data sets of different configurations, especially from electronic theories, cluster-expansion practitioners selected relevant ECIs in Eq. (1) on the basis of short-rangeness[34] and *ad hoc* spatial-decay of the ECIs criteria.[30] The associated expansion coefficients, that is, the effective cluster interactions, were determined by minimizing the least-squares fitting error

$$\Delta^2_{\mathrm{Fit}}=\frac{1}{N_s}\sum_i f_i\left(F_i-\sum_\alpha D_\alpha J_\alpha \Phi_\alpha(\boldsymbol{\sigma}_i)\right)^2, \tag{2}$$

for the input structures $i=1,\ldots,N_s$ and a set of N_c cluster figures $\alpha=1,\ldots,N_c$. The (constant) structure weights f_i allow one to give a certain structure, e.g., a ground state more weight.[35] The structure-inversion method of Connolly and Williams[34] corresponds to the special case when $N_s=N_c$ *and* Eq. (1) can be inverted. It has been shown,[30] however, that $N_s>N_c$ provides better ECIs.

With the advent of powerful and efficient computer resources, both hardware and software (band-structure codes), this original scenario has shifted toward a more heuristic approach where the selection of the cluster figures is done by minimizing the cross-validation score (CV):[31]

$$\Delta^2_{\mathrm{CV}}=\frac{1}{N_s}\sum_k f_k\left(F_k-\sum_\alpha D_\alpha J^{(k)}_\alpha \Phi_\alpha(\boldsymbol{\sigma}_k)\right)^2. \tag{3}$$

The CV score is the mean-square error for predicting F_k when the expansion is performed without taking configuration $\boldsymbol{\sigma}_k$ into account, for all N_s structures considered. For obvious reasons, this process has been also termed "leave-one out" cross-validation.[31]

Currently, the selection of the cluster figures is done based on a compactness criterion[31–33] or on the basis of an automated genetic-algorithm process.[36] The latter method illustrates what we meant by heuristic approaches. In their contribution, Hart and co-workers[36] used a genetic-algorithm approach, where the CV score is optimized by determining a small number ($\sim$5) of many-body cluster figures out of a pool of clusters ($\sim$50) generated on the basis of maximum bond length ($\sim$fifth nearest neighbor). Their results for bcc- and fcc-based systems showed that good CV scores can be obtained with a small number of cluster figures, some of them quite open.

B. Variational approach to the cluster expansion method

In this paper we have used a newly developed variational approach[27] to determine the relevant cluster figures in the cluster expansion. A good way to present the method is to consider the following question: How to know if a given set of cluster figures produces indeed the lowest prediction error? This is an important question because we will always have finite (limited) amount of input data from which we would like to get the best expansion possible. And by the "best expansion" we mean a physically transparent and numerically efficient expansion that produces the smallest possible fitting and prediction errors. We have proposed an effi-

cient algorithm based on weighting the expansion coefficients in Eq. (2). The new objective function then takes the form

$$\Delta^2_{\mathrm{Gen}} = \frac{1}{N_s - 1}\left(\sum_{i \neq k}^{N_s - 1} f_i \left(F_i - \sum_{\alpha} D_\alpha J^{(k)}_\alpha \Phi_\alpha(\boldsymbol{\sigma}_i) \right)^2 + \sum_{\alpha} D_\alpha w^2_\alpha J^2_\alpha \right). \quad (4)$$

The optimum value of the weights is determined from the minimization of the average prediction error

$$\frac{\partial \Delta^2_{\mathrm{CV}}}{\partial w_\alpha} = \frac{\partial}{\partial w_\alpha}\left[\frac{1}{N_s} \sum_k f_k \left(F_k - \sum_\alpha D_\alpha J^{(k)}_\alpha(\boldsymbol{w}) \Phi_\alpha(\boldsymbol{\sigma}_k) \right)^2 \right] = 0, \quad (5)$$

for all clusters α. We have written $J^{(k)}_\alpha(\boldsymbol{w})$ to emphasize that the ECIs are now functions of the weights. In practice, this optimization strategy selects the relevant clusters by assigning them low weights and discarding clusters that do not contribute to a stable expansion by associating them with large weights. The most important characteristic of our method is that the process of sorting out irrelevant clusters is driven by the optimization of the cross-validation error in a variational way. Another relevant aspect of our method is that both weighted fitting and prediction errors always decrease with the number of clusters, contrary to the traditional cross-validation score.[27]

It is obvious that the minimization of Δ^2_{CV} in Eq. (5) cannot yield useful results if too many cluster figures are used to fit a given set of input data, i.e., $N_c > N_s$. In order to complete Eqs. (4) and (5) an optimization strategy is required that judges the stability of the cluster expansion coefficients. This is achieved by systematically removing clusters from the expansion and monitoring the stability of the expansion coefficients. The simplest sort-out mechanism consists of removing the cluster with the lowest value of $|D_\alpha J_\alpha|$ after the weights have been optimized, and then minimizing Δ^2_{CV} again [Eq. (5)]. This procedure is repeated until the prediction error of the reduced pool starts to increase more than a certain numerical value. Then a significant cluster figure was removed. At this stage the sorting-out procedure can still be continued to further decimate the number of clusters at the expense of a larger prediction error.

C. First-principles calculations of selected ordered Fe and Co structures

The *ab initio* calculations of the enthalpy of formation, atomic volume, and magnetic moment (the F's in Sec. II A for Fe-Co alloys were performed using a mixed-basis plane-wave pseudopotential (MBPP) implementation as encoded in the Stuttgart package.[37] The MBPP code is particularly well suited for describing the electronic properties of transition metals and their alloys, since the approach successfully combines the merits of plane-wave pseudopotential methods with an atomic-like basis—that handles the narrow-band electronic states with few localized functions. This characteristic makes the MBPP computationally efficient, since few plane waves are needed to provide converged results. For our present calculations of Fe, Co, and their alloys, we have used a plane-wave energy cut-off $E_{\mathrm{pw}} = 18$ Ry and five local orbitals of d symmetry per atom. The local orbitals were constructed by trimming the respective atomic pseudowave function beyond a cut-off radius of 2.0 bohr for both Fe and Co atoms. This muffin-tin radius is well below the touching-spheres limit, thus allowing for structural relaxations in Fe-Co alloys. Also, we have used norm-conserving, nonlocal pseudopotentials[38] including a nonlinear partial-core correction for the exchange and correlation contribution,[39] which is very important in treating spin-polarized systems.

In all the calculations we used a generalized gradient approximation (GGA) to the exchange and correlation energy as proposed by Perdew, Burke, and Ernzerhof.[40] The electron densities were calculated in a Fourier representation enclosing plane waves up to 900 Ry. The k-point mesh integration was carefully done using a special set of points as provided by the Moreno-Soler scheme[41] together with a Gaussian broadening of 7 mRy. Using an equivalent set of k points guarantees the best possible cancellation of errors when computing enthalpies of formation. Besides, it has been shown that equivalent k-point convergency is faster than absolute convergency.[30] A grid of $16 \times 16 \times 16$ k points for the body-centered cubic (bcc) unit cell was used in all calculations or denser when this k-point mesh was incommensurate with the periodicity of the structure. With the above-mentioned parameters, enthalpies of formation were numerically converged to within 0.1 mRy/atom. In Table I we show our MBPP-GGA results for equilibrium atomic volume and the magnetic moment for Fe and Co in a bcc structure, together with results of previous calculations found in the literature. Experimental data are quoted where available.

Our MBPP-GGA results compare very well with previous first-principles calculations and experimental results. The energy difference between the nonmagnetic and the spin-polarized solution (E_{mag}) in Fe bcc also shows sizable variations that might be ascribed to the promotion of the $3p$ states as semicore states. This is reflected in a slightly smaller atomic volume and magnetic moment. On the other hand, the discrepancy between the experimental and the predicted magnetic moment for bcc Co is not due to computational approximations but due to other factors.

Cobalt occurs naturally in an hexagonal close-packed structure that changes into a face-centered cubic lattice upon raising the temperature above 427 °C. Body-centered cubic Co is not found in nature. However, after its experimental realization by Prinz as thick films on GaAs substrate,[61] bcc cobalt drew a great deal of attention from the theoretical community, especially on its mechanical[56] and magnetic[55,56,58–60] properties—the first band-structure calculations on bcc-Co were performed by Callaway and co-workers,[62] using a linear combination of Gaussian orbitals method. All these calculations (see Table I) predicted a magnetic moment of about $1.7\mu_B$ in contrast to the experimental measurements of $1.5\mu_B$. Although initially it was believed that substrate strain effects were responsible for such a low value of the magnetic moment, later experimental[63] as well as theoretical[64] evidence pointed toward contamination as

TABLE I. Structural and magnetic properties of bcc Fe and Co obtained in this paper and compared with previous first-principles calculations and experimental measurements. All calculations were performed using GGA for the exchange and correlation (xc) potential with the exception of those using the von Barth-Hedin (vBH) functional. Perdew and Wang GGAs are denoted by PW86 (Ref. 42) and PW91 (Ref. 43). NCPP and USPP denote norm-conserving and ultrasoft pseudopotentials, respectively. Projector augmented wave (PAW) results from VASP (Ref. 44). E_{mag} is the difference between the nonmagnetic and the ferromagnetic total energies.

Metal	Method	XC type	V (a.u.^{3})	M_0 (μ_B)	E_{mag} (mRy/atom)	Ref.
Fe	MBPP	PBE	79.6	2.32	44.0	This work
	MBPP	PBE	79.3	2.27	43.8	45
	MBPP	PW86	87.8	2.35	46.0	46
	MBPP	PW86	84.1	···	41.0	47
	LAPW	PW86	80.7	2.13	35.1	48
	LAPW	PW91	76.8	2.17	···	49
	LAPW	PW91	77.2	2.17	33.9	50
	LMTO	PW91	77.0	2.24	28.7	51
	NCPP	PW91	78.7	2.32	38.0	52
	USPP	PW91	79.0	2.32	40.6	53
	PAW	PW91	76.6	2.20	32.8	54
	Exp.	···	79.5	2.22	···	3
Co	MBPP	PBE	76.8	1.77	29.6	This work
	LAPW	vBH	69.5	1.62	···	55
	LAPW	vBH	71.0	1.73	23.0	56
	LAPW	PW91	76.5	1.74	···	57
	LMTO	vBH	75.3	1.73	11.0	58
	ASW	vBH	74.0	1.68	···	59
	PAW	PW91	74.5	1.69	···	60
	Exp.	···	75.7	1.53	···	61

the source for the low magnetic moment in bcc cobalt.

The magnetic and mechanical properties for selected Fe-Co ordered structures as calculated in the MBPP are presented in Table II. Contrary to the pure elements, theoretical investigations are less abundant and mostly focused on predicting the magnetic moment. Experimental information is also scarce especially for the mechanical properties. The available theoretical results for the B2 phase (CsCl-type) of Fe-Co are consistent among themselves, showing an atomic volume within few percent of the experimental value. The data show the well-known features of GGA and the local-density approximation (LDA) when applied to magnetic systems, that is, LDA predicts smaller atomic volumes and low values for the magnetic moment. The GGA corrects some of the overbinding of the LDA but, in general, overestimates the magnetic energy, predicting higher magnetic moments. The enthalpy of formation ΔE, i.e., the energy of a given configuration referred to that of the concentration-weighted average of the pure components, for the B2 phase is −9.3 mRy/atom, which agrees well with our projector augmented wave (PAW) calculations. In the case of the B32 (NaTl-type) and the $D0_3$ (Fe_3Al-type) structures, we also found a negative enthalpy of formation indicating an ordering tendency in this system. The comparison in Tables I and II, albeit brief, provide a measure of the reliability and accuracy of the MBPP first-principles calculations in Fe-Co alloys (see Sec. III).

TABLE II. Structural and magnetic properties of selected bcc Fe-Co alloys obtained in this paper and compared with previous first-principles calculations and experimental measurements.

Structure	Method	XC type	V (a.u.^{3})	M_0 (μ_B)	ΔE (mRy/atom)	Ref.
FeCo-B2	MBPP	PBE	79.7	2.29	−9.3	This work
	PAW	PBE	78.0	2.25	−8.0	This work
	LAPW	PBE	77.6	···	···	26
	LAPW	PW86	71.8	2.25	···	17
	LMTO	VWN	···	2.27	···	24
	ASW	vBH	76.2	2.18	···	18
	ASW	vBH	75.3	2.21	···	15
	Exp.	···	78.8	2.40	···	3
Fe_2Co_2-B32	MBPP	PBE	79.3	2.22	−4.5	This work
	PAW	PBE	77.5	2.17	−3.4	This work
	ASW	vBH	75.2	2.15	···	15
Fe_3Co-$D0_3$	MBPP	PBE	80.0	2.36	−6.2	This work
	PAW	PBE	78.4	2.32	−5.0	This work
	ASW	vBH	76.0	2.30	···	15
$FeCo_3$-$D0_3$	MBPP	PBE	78.1	2.00	−3.4	This work
	PAW	PBE	76.4	2.00	−2.7	This work
	ASW	vBH	75.1	1.90	···	15

III. RESULTS

We used the mixed-basis plane-wave pseudopotential method described in Sec. II C to calculate the enthalpy of formation and the magnetic moment of a set of 68 Fe_nCo_m ordered structures. The atomic volume was obtained from the fit of the Vinet equation of state[65] to the calculated data. For each structure, all the crystal parameters were relaxed, either by minimizing the total energy against the proper distortion, e.g., volume and the c/a ratio, or by minimizing the forces on the atoms with positions not fixed by symmetry. The atomic positions were relaxed using the Broyden-Fletcher-Goldfarb-Shanno (BFGS) method,[66] achieving an accuracy of 1 mRy/a.u. Table III summarizes the results of the calculations. Note that when a structure has a known *Strukturbericht* designation symbol we have listed it in the table next to the corresponding stoichiometry. Further details of the crystal structures of the calculated Fe-Co compounds are found in the Appendix.

The enthalpy of formation ΔE, i.e., the energy of a given configuration referred to that of the concentration-weighted average of the pure components,

$$\Delta E(\boldsymbol{\sigma}) = E(\boldsymbol{\sigma}) - xE(\mathrm{Fe}) - (1-x)E(\mathrm{Co}), \qquad (6)$$

is negative for all structures considered, indicating a strong tendency for ordering in Fe-Co alloys. Spin-polarization is

TABLE III. Atomic volume, average magnetic moment, and enthalpy of formation, of ordered bcc-based Fe-Co structures calculated with the MBPP using the GGA-PBE for the xc potential. The last column stands for the enthalpy of formation obtained when the spin polarization is not considered. The enthalpy of formation of the Fe-rich ground states predicted by the cluster expansion is shown between parentheses.

Composition	Structure	Volume (a.u.^{3})	M_0 (μ_B)	ΔE (mRy/atom)	ΔE_{nsp} (mRy/atom)
$Fe_{15}Co$	$Fe_{15}Co$	80.10	2.382	−1.77 (−1.84)	48.39
Fe_7Co	(100) SL	80.29	2.414	−3.33	47.84
	Fe_7Co	80.16	2.392	−3.53 (−3.64)	47.75
Fe_6Co	(100) SL	80.30	2.405	−3.92	47.59
	Fe_8CoFe_4Co-(100) SL	80.20	2.393	−3.90	47.46
$Fe_{13}Co_3$	$Fe_{13}Co_3$	80.25	2.394	−5.19 (−5.16)	47.00
Fe_4Co	(100) SL	80.25	2.392	−5.43	46.90
Fe_3Co	$D0_3$	80.00	2.360	−6.19	45.65
	$L6_0$	80.06	2.364	−6.52 (−6.63)	46.00
	(100) SL	80.15	2.376	−6.46	45.98
	Fe_6Co_2-(100) SL	80.06	2.345	−3.46	45.58
	$Fe_3CoFeCoFe_2$-(100) SL	80.23	2.381	−5.94	46.16
Fe_5Co_2	(100) SL	79.98	2.332	−4.04	44.93
	Fe_3CoFe_2Co-(100) SL	80.16	2.377	−7.08	45.42
$Fe_{11}Co_5$	$Fe_{11}Co_5$	79.86	2.331	−7.61 (−7.67)	44.90
	$Fe_2Co(Fe_3Co)_2Fe_2CoFeCo$-(100) SL	80.13	2.368	−7.23	45.09
Fe_2Co	C11b	80.15	2.364	−7.59	44.71
	$(FeCo)_2Fe(FeCo)_2Fe_3$-(100) SL	80.11	2.359	−7.35	44.91
	Fe_8Co_4	79.87	2.330	−7.96	44.67
Fe_5Co_3	Pd_5Ti_3	80.03	2.344	−7.99	44.08
	(100) SL	79.53	2.257	−3.24	43.09
	$Fe_2Co_2FeCoFe_2$-(100) SL	79.73	2.285	−5.83	43.52
	Fe_5Co_3	79.89	2.331	−8.67 (−8.67)	44.17
Fe_3Co_2	Al_3Os_2	79.93	2.323	−8.16	43.75
	(100) SL	79.70	2.281	−5.07	43.01
Fe_4Co_3	Cu_4Ti_3	79.60	2.274	−6.49	42.39
	$(FeCo)_3Fe$-(100) SL	79.83	2.310	−8.48	43.24
	(100) SL	79.39	2.233	−3.72	42.00
Fe_9Co_7	Fe_9Co_7	79.82	2.311	−9.10 (−9.09)	43.29
Fe_5Co_4	V_4Zn_5	79.51	2.252	−5.58	42.11
	$((FeCo)_3Fe)_2Fe(FeCo)_2$-(100) SL	79.85	2.309	−8.66	43.17
FeCo	B2	79.70	2.289	−9.32 (−9.46)	42.40
	B32	79.29	2.217	−4.49	40.81
	B11	79.33	2.214	−5.77	41.06
	Fe_4Co_4-(100) SL	79.04	2.170	−3.28	40.65
	$Fe_2Co_2(FeCo)_2$-(100) SL	79.49	2.241	−7.55	41.62
	$Fe_3CoFeCo_3$-(100) SL	79.25	2.208	−5.41	41.12
Fe_4Co_5	V_4Zn_5	78.98	2.163	−4.63	40.06
	$((CoFe)_3Co)_2Co(CoFe)_2$-(100) SL	79.26	2.200	−8.55	40.75
Fe_7Co_9	Fe_7Co_9	79.23	2.206	−7.83	40.68
Fe_3Co_4	Cu_4Ti_3	78.89	2.139	−5.98	39.40
	$(CoFe)_3Co$-(100) SL	79.14	2.171	−8.27	40.19
	(100) SL	78.74	2.123	−3.57	39.11
Fe_2Co_3	Al_3Os_2	78.93	2.128	−7.61	39.38
	(100) SL	78.67	2.110	−4.23	38.72

TABLE III. (*Continued.*)

Composition	Structure	Volume (a.u.^{3})	M_0 (μ_B)	ΔE (mRy/atom)	ΔE_{nsp} (mRy/atom)
Fe_3Co_5	Pd_5Ti_3	78.85	2.112	−6.91	38.74
	(100) SL	78.55	2.085	−3.06	38.22
	$Co_2Fe_2CoFeCo_2$-(100) SL	78.68	2.109	−5.11	38.61
Fe_3Co_5	Fe_3Co_5	78.84	2.138	−6.53	39.31
$FeCo_2$	C11b	78.57	2.061	−5.96	37.55
	$(CoFe)_2Co(CoFe)_2Co_3$-(100) SL	78.60	2.082	−6.40	38.05
	Fe_4Co_8	78.58	2.090	−5.79	38.19
Fe_5Co_{11}	Fe_5Co_{11}	78.46	2.070	−5.26	37.77
	$Co_2Fe(Co_3Fe)_2Co_2FeCoFe$-(100) SL	78.47	2.057	−5.67	37.43
Fe_2Co_5	(100) SL	78.12	2.010	−3.17	36.32
	Co_3FeCo_2Fe-(100) SL	78.30	2.028	−5.17	36.69
$FeCo_3$	$D0_3$	78.11	2.001	−3.38	36.05
	$L6_0$	78.11	2.008	−4.08	36.46
	(100) SL	78.07	1.998	−4.31	36.05
	Fe_2Co_6-(100) SL	77.98	1.985	−2.71	35.74
	$Co_3FeCoFeCo_2$-(100) SL	78.12	1.998	−4.60	36.25
$FeCo_4$	(100) SL	77.74	1.940	−3.77	34.82
Fe_3Co_{13}	Fe_3Co_{13}	77.77	1.939	−2.97	34.45
$FeCo_6$	(100) SL	77.52	1.896	−2.52	33.65
	Co_8FeCo_4Fe-(100) SL	77.51	1.894	−2.61	33.75
$FeCo_7$	(100) SL	77.42	1.880	−2.25	33.52
	$FeCo_7$	77.43	1.886	−1.95	33.73
$FeCo_{15}$	$FeCo_{15}$	77.10	1.825	−0.94	32.35

fundamental in obtaining a correct description of the energetics of Fe-Co alloys,[16,20,26] as demonstrated by Fig. 1 and the last column in Table III, where we show the formation enthalpy ΔE_{nsp} when the spin-polarization has been switched off from the fully-relaxed magnetic results. In order to make the comparison meaningful, we have used the bcc ferromagnetic phases of Fe and Co as the standard states in both ΔE and ΔE_{nsp}. The difference between these two energies give us, in a first approximation, an estimation of the magnetic energy in Fe-Co alloys. Note that ΔE_{nsp} contains both the inter- and intra-atomic magnetic contributions to the total energy, explaining why it is several times larger than ΔE. We will return to this point later on.

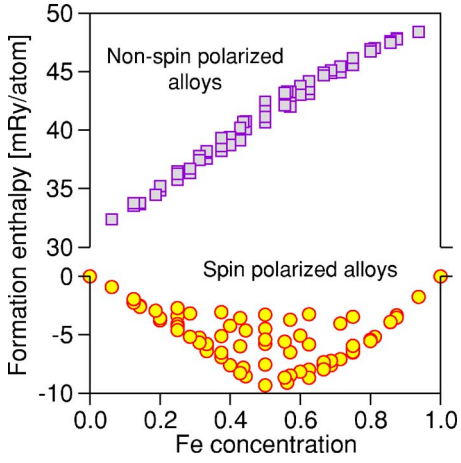

FIG. 1. (Color online) Enthalpy of formation of ferromagnetic (circles) and of paramagnetic (squares) Fe-Co alloys. The latter was obtained from the fully relaxed ferromagnetic case by switching the spin polarization off. Positive values of the enthalpy of formation describe phase-separating alloys whereas the opposite stands for ordering systems.

The relaxation effects are, in general, small in Fe-Co alloys, being more pronounced on the Co-rich side but usually of a few percent only. This is understandable since Fe and Co have very similar atomic sizes and electronic structures—they are neighbors in the periodic table. It also explains the success of simpler approaches such as the virtual crystal approximation in describing the magnetism of Fe-Co alloys.[19,20] Treating Fe-Co alloys as disordered systems for all temperatures and concentrations is a different issue, since there are no *a priori* indications that this might be the case. The cluster expansion technique, as presented in Secs. II A and II B, is an ideal tool to investigate this point because it allows for a direct comparison between the ordered and disordered states.[67] Since the disordered state of the alloy is calculated from the knowledge of the set of ordered structures (Table III), it has all virtues of the latter, including the relaxation contributions and the accuracy of the first-principles calculations.

We have cluster expanded the formation enthalpies of Fe-Co alloys of Table III, finding that a small set of 12 ECIs

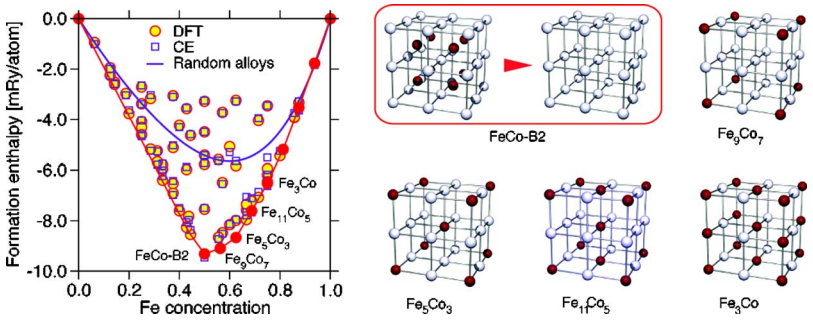

FIG. 2. (Color online) Enthalpy of formation of bcc-based Fe-Co alloys as obtained by first-principles total energy calculations (circles) and the cluster expanded energies using a set of 12 ECIs (squares). The fitting and prediction errors are 0.10 and 0.12 mRy/atom, respectively. The solid line stands for the enthalpy of formation of the random alloy. In order to emphasize that the new ground states are derivatives of a B2 motif, only the occupation for one sublattice is shown. The other sublattice is fully occupied with Fe atoms. This is illustrated for the B2 phase in the rounded rectangle.

is enough to describe the configurational aspect of the chemical bonding with an accuracy of 0.12 mRy/atom (prediction error). Figure 2 contains both the direct density-functional (DFT) and the cluster expanded (CE) formation enthalpies. The formation enthalpy of the random alloy is denoted by a solid line. Several features in Fig. 2 are worthy to be emphasized. First, the enthalpy of formation of the ordered compounds around equiatomic composition is almost twice as big as the corresponding enthalpy of the random alloy, pointing to short- and long-range order effects important for the configurational thermodynamics of Fe-Co. Second, the calculated enthalpies of formation reproduce the asymmetry observed in the experimental phase diagram,[4] showing stable ordered structures for the Fe-rich side. This is an interesting result, especially because the experimental phase diagram shows FeCo-B2 (CsCl) as the only ordered phase. According to our results, there are seven additional bcc-based Fe-rich ground-state structures. A third interesting characteristic of Fig. 2 is that Fe_3Co superlattices are stable in the form of a $L6_0$ structure, thus supporting the existence of such superlattices for Fe-Co. We did not find, however, stable bcc-based $FeCo_3$ superstructures. Let us comment on each of these points separately.

One of the great advantages of the cluster expansion technique is that once the expansion is converged (as judged by the fitting and prediction errors), one can straightforwardly predict the energy of *any configuration* with virtually no computational effort. This is a very useful fact when confronted with the possibility that a system might have new phases. We used the above-obtained ECIs to a direct enumeration ground-state (GS) search, where the enthalpy of formation of bcc-based supercells, of different shape and containing up to 32 atoms, was evaluated. Our combinatorial search resulted in 8 ground-states, out of the 1.5×10^{10} scanned configurations, for Fe-rich Fe-Co alloys. These GSs, depicted in Fig. 2 with closed circles, proved to be stable against phase separation into structures of neighboring composition. We also ascertained the existence of such new GS structures by directly calculating their enthalpy of formation using our first-principles total energy mixed-basis plane-wave pseudopotential method. What is really interesting is that these new GS structures appear every 1/16 in Fe concentration from the equiatomic alloy. The underlying mechanism is very appealing because of its simplicity and because it is related to the topology of bcc-based alloys.

A bcc lattice can be split into two equivalent simple cubic (sc) sublattices each containing half of the sites of the crystal: One sublattice is defined by the "body-centered" sites and the other simple-cubic sublattice is defined by the "cubic" sites. Because of this, frustration effects are not present in bcc-based systems with ordering (antiferromagnetic) interactions—as opposed to the face-centered cubic lattice. A strong nearest-neighbor pair interaction stabilizes the B2 (CsCl-like) phase. In terms of the two simple-cubic sublattices, the B2 structure can be viewed as having each atomic species occupying exclusively one sublattice. The obtained ECIs for the Fe-Co alloys show a nearest-neighbor pair interaction that is almost an order of magnitude larger than any of the other ECIs. This makes the B2 phase stable enough to "lock" the Fe atoms to one of the simple-cubic sublattices. Thus, an increase in the Fe concentration will only affect the atomic distribution in the other sublattice. A simple inspection of the structures in Fig. 2 shows that this is indeed the case. We can then simplify the picture by transforming the bcc-based ECIs into sc-based ECIs by subsuming the occupancy of the locked Fe atoms. This effectively reduces the dimensionality of the interactions in that n-body ECIs are transformed into $(n-m)$-body interactions, when the original cluster figure contains m sites in the Fe sublattice. The reduced effective cluster interactions (RECIs) obtained in this way (not shown) have pair and three-body interactions. Although the reduced three-body interactions are necessary to capture subtle details of the ground-state phase diagram, like its asymmetry with concentration, the key parameters are the reduced effective pair interactions (REPIs). In the case at hand, all REPIs are positive except the sixth one that is zero. This is the key to the periodicity of the GS structures, because the sixth REPI sets the characteristic length between Fe atoms in the unlocked sublattice. In other words, upon increasing the Fe concentration from 50%, the Fe atoms occupy positions in the sc lattice so that unlike atoms are $2a$ (the length of the sixth REPI) apart from each other. This motif is complete when the nominal concentration is $x=9/16$, thus stabilizing the Fe_9Co_7 GS. Further increase of the Fe concentration will fill the remaining sc sites according to remaining positive RECIs, subject to the supercell size in steps of 1/16.

In a previous investigation on the ground states of Fe-Co alloys,[10] we found that the sixth REPI became negative thus setting the characteristic length scale of the ground-state sequence. From the general argument of Ref. 10, it is clear that for the determination of ground-state sequence, having a negative REPI among a positive distribution (i.e., a local minimum) is equivalent to having such REPI as the last one and with zero value. There are two main reasons for having this change in the value of the sixth REPI. Primarily, we have increased our input-structure database by 48%, that is, from 46 to 68 structures. Second, we have considerably improved our algorithm to select the relevant cluster figures in the expansion, so that our current fitting and predicted errors are almost threefold smaller than previously. Since the details of ECIs (and therefore the RECIs) depend on these two aspects, it is no surprise to find small quantitative changes. However, the physical picture remains the same, as we have already shown. A more complicated REPI behavior, e.g., oscillating chemical and weak yet long-ranged elastic interactions, can induce a continuous succession of adaptive crystal structures.[68,69]

The experimental Fe-Co phase diagram shows an asymmetric order-disorder boundary where the transition temperature is higher for Fe-rich alloys.[4] Our first-principles calculations for the enthalpy of formation reflect this characteristic, i.e., Fe-rich alloys have large values of the enthalpy of formation. The fact that most of the Co-rich bcc-based alloys are above the tie line indicate that such compounds are not likely to be formed in a bcc-like environment. This is again in agreement with the experimental observation of Co-rich alloys crystallizing in close-packed structures.[3] Actually, it is in this region where the atomic relaxations are more accentuated but still of a few percent. The virtual crystal approximation (VCA) assumes an alloy volume that interpolates linearly between the atomic volumes of the pure elements (Vegards's law). Considering the success of the VCA in the description of the magnetism in Fe-Co alloys,[19,20] one would expect that the atomic volume should follow Vegard behavior. However, our results show that the atomic volume depends on the atomic concentration in a nonmonotonic fashion, deviating from Vegard's law. Figure 3 contains our first-principles calculations for the atomic volume as function of the Fe concentration for both ordered and disordered alloys—the latter calculated via a cluster expansion. It is interesting to observe that the atomic volume depends strongly on the concentration and that is only slightly sensitive to the configurational degrees of freedom.

We attribute the overestimation of the atomic volume to the overestimation of the magnetic energy, a known behavior of the GGA functionals.[72] Nevertheless, it is gratifying to see that such overestimation occurs in a systematic way, locating our first-principles GGA-PBE predictions within 2% of the experimental values in all the concentration range. In Fig. 3 we show the results of Rodgers and Maddocks[70] that measured the atomic volume of Fe-Co alloys after slow cooling the samples from 600 to 650 °C (squares). Ellis and Greiner[71] reported the atomic volume after quenching the samples from 575 to 580 °C (triangles) and 800 °C (inverted triangles) down to 25 °C. The atomic volume shows a slight increase upon ordering around equiatomic

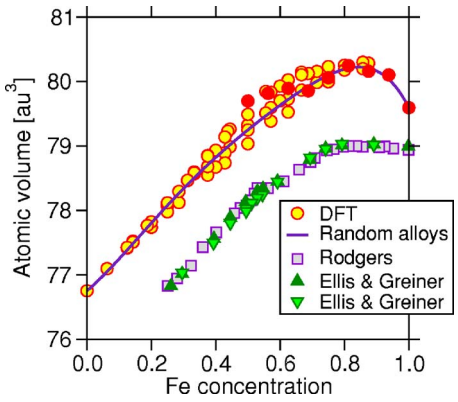

FIG. 3. (Color online) Calculated first-principles GGA-PBE atomic volume of Fe-Co alloys as function of the Fe concentration. Experimental data from Rodgers—Ref. 70 (squares) and Ellis and Greiner—Ref. 71 (triangles: quenched samples from 575 to 580 °C, inverted triangles: quenched samples from 800 °C). The atomic volume of the ground-state structures is marked with closed circles. See the text.

composition,[71] a trend that is very well reproduced by our theoretical data (see also Table III). In general, the atomic volume of a binary alloy shrinks upon ordering. In the case of Fe-Co alloys occurs the opposite because of the magnetism (see the following).

In Fig. 4 we show our *ab initio* results for the magnetic moment in ordered and disordered Fe-Co alloys, together with the experimental values obtained by Bardos[73] in both fast-quenched (disordered) and slow-cooled (ordered) samples. Our theoretical predictions and the actual values for the magnetic moment per atoms agree well. Different from the case of the atomic volume, however, the discrepancy between the experimental and the theoretical values is not systematic. At large Fe concentrations the first-principles results overestimate the magnetic moment, whereas the oppo-

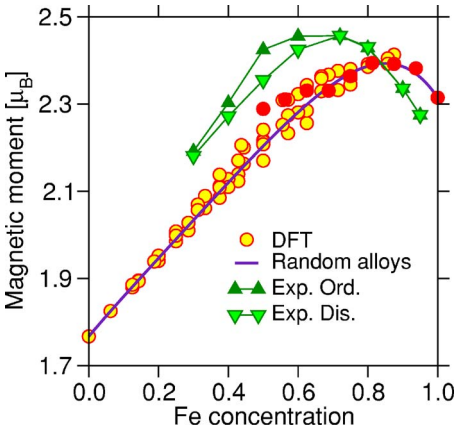

FIG. 4. (Color online) Calculated first-principles GGA-PBE magnetic moment per atom as a function of the Fe concentration for bcc-based Fe-Co alloys. Circles stand for the set of 68 ordered structures of Table II, while the solid line represents the magnetic moment of the random alloy. Experimental data are presented for ordered (inverted triangles) and disordered (inverted triangles) alloys from Bardos (Ref. 73). See the text.

site happens at low Fe concentrations. This discrepancy is by no means associated to a particular method of calculation, since it is present in all first-principles approaches (see, for example, the FeCo-B2 entry in Table II). One might think that a possible explanation to this discrepancy comes from the fact that we had ignored the orbital contribution to the magnetic moment. However, the experimental observations of Reck and Fry attribute the orbital polarization only to 4%–5% of the total magnetic moment of bcc-based Fe-Co alloys.[74] First-principles calculations within the virtual-crystal approximation also showed a uniform increase of few percent in the total magnetization when the orbital contribution, both in the form of spin-orbit and orbital polarization, was taken into account.[20] Recent exact muffin-tin-orbital calculations in Fe-Co alloys, where the one-electron effective potential was represented by the optimized overlapping muffin-tin potential[75] and the disorder was modeled within the coherent-potential approximation,[76] are also in agreement with the VCA and experimental results. Clearly, a uniform upward shift in the magnetic moment per atom would improve the agreement around equiatomic composition but would make it worse for Fe-rich alloys.

A possible source for this discrepancy might be found in the inherent limitations of the local-density (LDA) and GGA to deal appropriately with local quantities that are related to the spin polarization. Although the GGA generally improves integral quantities such as the total ground-state energy over LDA, it is less successful in improving local quantities like the difference between spin-up and spin-down in the exchange potentials.[77] Experimentally, some of these restrictions have been pointed out by neutron scattering measurements on FeCo single crystals.[78] The GGA-PBE functional used in this paper is considered the best in its class for solid state properties.[79] To resolve the issue of electronic and spin distributions in Fe-Co alloys, it might be necessary to go beyond the GGA, i.e., to use a meta-GGA such as the Tao-Perdew-Staroverov-Scuseria,[80] that is a semilocal functional on the density and the occupied orbitals. Such an analysis, although interesting *per se*, is beyond the scope of the present contribution.

IV. DISCUSSION

A. Magnetic moment and equilibrium volume in Fe-Co alloys

It is well known that a rigid-band picture is inadequate to explain the dependence of the magnetic moment with concentration in Fe-Co alloys.[13] Williams *et al.*[81] suggested that the magnetic moment versus concentration curve is defined by the interplay between strong ferromagnetism (for the Co-rich side of the maximum) and weak ferromagnetism (for the Fe-rich side). This ferromagnetic weakness coincides with a pinning of the Fermi level at the valley of the minority density of states. However, an *spd* tight-binding Hamiltonian by Victora and Falicov[19] pointed to electron-electron correlations as the source for the anomalous shape of the magnetic moment versus concentration curve. Within their theory, the maximum of the magnetic moment curve is indeed due to strong ferromagnetism for Co-rich alloys, as Williams *et al.*[81] had suggested, until the addition of Fe causes electronic correlations, now insufficient to cause saturation, to become more important. The transition from weak (Fe-rich) to strong (Co-rich) ferromagnetism is driven by an occupation of the Fe minority spin band as the concentration of Co is increased and the subsequent shift of *d* levels. The Coulomb interaction is responsible for this shift and affects both spin-up and spin-down levels equally. An occupation of the majority band thus increases the magnetic moment of the alloy. Figure 4 shows a maximum of the magnetic moment located at higher Fe concentration than the experimental results. As outlined in the previous section, we believe that this discrepancy can be attributed to electronic correlations, i.e., it is necessary to go beyond the GGA, for example, by using the meta-GGA of Tao-Perdew-Staroverov-Scuseria[80] that is a semilocal functional on the density and the occupied orbitals. Certainly more theoretical work is needed and we hope that the present contribution motivates some of it.

On the other hand, note that the magnetic moment does not change significantly upon ordering, i.e., magnetism in Fe-Co alloys is not very sensitive to the configurational degrees of freedom but dominated by the concentration. This explains the success of approaches as the virtual crystal (VCA)[19,20] or the coherent potential approximation (CPA)[21–25,76] in describing the dependence of the average magnetic moment with concentration. In the VCA, the Hamiltonian of the two constituent elements is coarse-grained to produce a concentration-averaged atom. Thus a binary alloy is modeled by this single-atom system in a lattice with the full symmetry of the disordered system. One would expect the VCA to render a good approximation when the elements are analogous in their electronic properties. Fe and Co are adjacent in the periodic table with very similar electronic properties, i.e., similar band widths and a large *d* occupation.

Interestingly enough, most of the VCA calculations for Fe-Co assumed an average atomic volume that follows Vegard's law, i.e., a linear interpolation between the atomic volumes of the pure elements. Our results in Fig. 3 show a positive departure from the linear behavior that resembles the behavior of invar alloys, i.e., the atomic volume reaches a maximum as a function of the concentration.[82] In this light, the VCA results give the impression that structural details, e.g., the atomic volume, do not have much bearing on the magnetic properties of Fe-Co alloys. However, the above discussion on the magnetism of Fe-Co alloys shows an interdependence between the atomic volume and the average magnetic moment, i.e., both are controlled by the relative occupation of the majority and minority bands as the concentration is varied.

Owing to the fact that both the equilibrium magnetic moment and the atomic volume of Fe-Co alloys show a remarkable similar dependence with atomic concentration, one can entertain the idea that the same mechanism that explains the maximum of the magnetic moment curve applies as well to the atomic volume. We based our argument on Pauling's[83] idea of separating the valence electrons into the "bonding" and "atomic" ones—Pauling actually called them bonding and atomic *orbitals*—with the former participating actively in bond formation whereas the latter are responsible for the magnetic moment. The precise definition of either type of

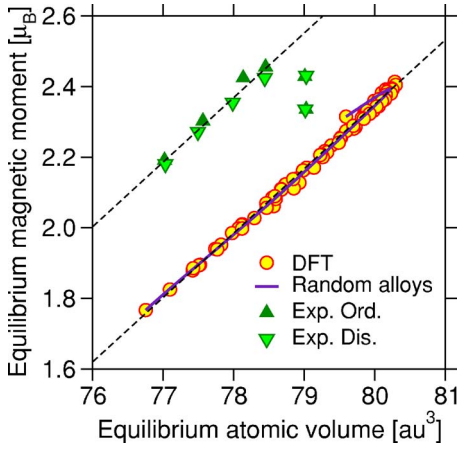

FIG. 5. (Color online) Equilibrium magnetic moment (m_0) as a function of the equilibrium atomic volume (v_0) for Fe-Co alloys. First-principles DFT calculations for ordered structures are represented by circles. The solid line stands for the fully disordered alloy. Experimental results (triangles) from Ellis and Greiner (Ref. 71) and Bardos (Ref. 73). See the text for further information.

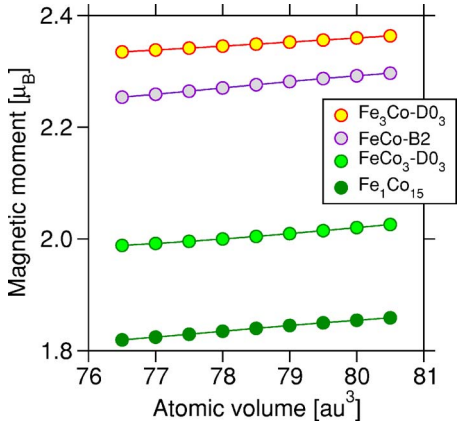

FIG. 6. (Color online) Calculated volume dependence of the magnetic moment for Fe_3Co-$D0_3$, FeCo-B2, $FeCo_3$-$D0_3$, and $FeCo_{15}$ ordered alloys. The average slope of the magnetic moment with atomic volume is ~0.01.

electrons has changed over the years though. Pauling used a rather simplified way to discriminate atomic from bonding electrons, basically because he had scarce experimental data, thus he obtained a very simple curve (a triangle in his case) for the magnetic moment versus band filling. The *magnetic valence* concept of Williams and co-workers provides a more accurate definition of the "atomic" electrons, thus reproducing more accurately the experimental data for several binary transition-metal alloys.[81] Therefore, one can rationalize the shape of the atomic volume versus concentration curve in terms of "atomic" electrons, that is, when passing from Fe to Co, the electronic concentration changes in such a way that all the electrons that contribute to the formation of the magnetic moment do not contribute to the bonding.

Figure 5 condenses Fig. 4 and Fig. 3 by plotting the equilibrium values of the magnetic moment (m_0) as function of the atomic volume (v_0) for Fe-Co alloys. It is remarkable to see that a linear relationship

$$m_0^{\mathrm{DFT}} = -12.229 + 0.18223 v_0^{\mathrm{DFT}} \tag{7}$$

develops between those two quantities, independent of the degree of configurational order—the first-principles data for ordered structures (circles) and the cluster expanded result for the fully disordered alloys (solid line) essentially have the same slope. In Fig. 5 we can see an upturn of the magnetic moment when the volume is around 80 a.u.^{3} for both the ordered and disordered alloys. This region corresponds to the Fe-rich alloys and, as is well known, Fe and Fe-rich alloys show anomalous behavior in their magneto-volume properties,[84] and the upturn is just a reflection of that.

Interestingly enough, our *ab initio* calculations show great consistency with experimental results. In Fig. 5, we have plotted (triangles) the magnetic moment reported by Bardos[73] as a function of the atomic volume from Ellis and Greiner[71] whenever both measurements were performed at the same concentration. The turn of the magnetic moment for large volumes is also present in the experimental data, although in a different direction. A linear fit of the experimental data (without the two points at large volumes) reveals a slope that is virtually the same of that obtained from the calculated data, i.e.,

$$m_0^{\mathrm{exp}} = -11.882 + 0.18270 v_0^{\mathrm{exp}}. \tag{8}$$

A skeptical reader might argue that a linear fit should be expected when the magnetic moment is fitted over such a small volume interval. We have checked this by performing *ab initio* calculations for the magnetic moment in the Fe_3Co-$D0_3$, FeCo-B2, $FeCo_3$-$D0_3$, and $FeCo_{15}$ structures in the same volume interval of Fig. 5. We found that the magnetic moment behaves linearly with volume but with a very small slope (~0.01), i.e., the magnetic moment varies slowly with volume (see Fig. 6). However, there are significant differences between Figs. 5 and 6. The former corresponds to the *equilibrium* values of both the magnetic moment and the atomic volume, whereas the latter is just a variation of the atomic volume around its equilibrium value.

The existence of such linear dependence between the atomic volume and the magnetic moment [either Eq. (7) or Eq. (8)] clearly points out that the magnetic moment in Fe-Co alloys depends only on the electron count, and not on other factors such as the configurational order. It also seems to corroborate the idea of "atomic" and "bonding" electrons explained above. From a practical point of view, on the other hand, having such a simple relation between m_0 and v_0 might be useful for experimentalists to fine-tune the magnetic moment by selecting the appropriate atomic volume (lattice constant).

B. Strain effects and A_3B superlattices in Fe-Co

One of the core results of the present contribution is that bcc-based Fe-Co alloys display a series of ordered ground-state structures for Fe-rich compounds (see Fig. 2). This is an interesting result for bcc-based systems in general, because the mechanism behind the dense sequence of GS structures is

due to the properties of the bcc lattice. However, it is also important for Fe-Co alloys in particular, because of the possible existence of Fe_3Co and $FeCo_3$ superlattices.[5–9] Our first-principles calculated enthalpies of formation for Fe-Co alloys (see Table III) show that Fe_3Co alloys have a stable $L6_0$ (Ti_3Cu-type) ground state. The Fe_3Co-$L6_0$ structure is very close in energy to several of its allotropic forms, including the $D0_3$ (Fe_3Al-type) and some (001) superlattices. This is a clear indication that the Fe-Co system has a tendency to form ordered structures with 3:1 stoichiometry on the Fe-rich side.

It is important to emphasize that central to the existence of a dense sequence of ordered structures in Fe-Co alloys, and in particular to the presence of Fe_3Co superstructures, is the idea of a nonrandom distribution of Fe atoms on the Co sites for Fe-rich alloys. Although derived from a pure theoretical basis, this idea has some experimental support from ^{59}Co nuclear magnetic resonance (NMR) investigations of the short-range order in bulk Fe-Co alloys.[85] In their investigation, Jay and co-workers[85] found that Co and Fe are not randomly distributed in the mixed sublattice of the Co-rich samples. They also found that such samples tend to segregate (in agreement with the experimental phase diagram), thus strengthening the B2 ordering in off-stoichiometric compounds.

On the other hand, we did not find stable $FeCo_3$ structures with an underlying bcc lattice, i.e., all calculated and searched configurations lead to structures with an enthalpy of formation above the tie line. This is in agreement with experimental measurements that report a two-phase (bcc+fcc) region for Co-rich alloys.[3,4] Notwithstanding that the investigation of the coexistence of different phases at low temperatures for Co-rich alloys is beyond the scope of this paper, preliminary calculations for $FeCo_3$ ordered alloys showed a gain in stability of the fcc-based phase that is sufficient to locate their formation enthalpy below the tie line. Considering that some of the fcc-based ordered structures can be viewed as a tetragonal distortion of a bcc-based phase, e.g., the $L1_0$ is related to the B2 phase, one can speculate if such ordered phases could be observed in epitaxial Fe-Co alloys.

Recently, Wojcik and co-workers[9] prepared Fe-Co thin films by molecular-beam epitaxy on MgO and GaAs substrates. X-ray diffraction showed that the bcc stability limit is shifted to Fe concentrations as low as 0.11, in contrast with bulk measurements that located the bcc-boundary around 0.25. For Fe concentrations lower than 0.11 the system displayed a sharp transition toward the fcc phase. Nuclear magnetic resonance measurements on a 1000-Å-thick $Fe_{0.27}Co_{0.73}$ sample deposited at 500 °C signaled a highly ordered structure where all Co atoms have the same environment. This observation led Wojcik *et al.* to conclude that a new ordered phase with stoichiometry close to $FeCo_3$ exists, although the stabilization mechanism could not clearly be elucidated from their experiments. The authors envisaged epitaxial strains or surface diffusion as the most probable ones. Our own *ab initio* calculations support that epitaxial strains may change the delicate hierarchy in the energies of competing structures as compared to our bulk materials.

C. Dense sequence of ground states, confinement effects, and nanostructured Fe-Co alloys

The fact that strain effects can stabilize phases not present in bulk alloys has a venerable history.[61,86] The underlying idea, independent of the details of the system, is that an "external field" stabilizes a phase that exists in the neighborhood of the RTP state of a material. In the case of the bcc cobalt[61] surveyed in Sec. II C and in the experiments of Wojcik *et al.*,[9] reviewed earlier, the external field is the epitaxial strain. Pressure and temperature, on the other hand, can also be used to access otherwise nonstable phases, e.g., fcc and hcp Fe.[87] The external fields are spanning a hypersurface, where all the possible phases are represented by local minima. At room temperatures and pressures, one of these minima develops as the global minimum thus defining the stable phase of a material for such conditions.

Confinement effects encompass both surface and finite-size effects that can be used to stabilize new phases.[88,89] The recent development of nanostructured intermetallics, single or multiphase polycrystalline solids with grain sizes in the range of few nanometers, usually exhibit properties that are significantly different from and often improved over their coarse-grained bulk counterparts.[90] Interfacial and finite-size effects are in consequence important to define the properties of such nanostructured alloys. Very recently, superlattices of air-stable Fe-Co nanoparticles were synthesized in solution from an organometallic precursor. The 15 nm FeCo nanoparticles adopted an unusual short-range atomic ordering that transformed into bcc upon annealing at 500 °C.[91] This nanostructured Fe-Co material proved to be homogeneous with excellent magnetic properties.

The dense sequence of ordered structures might have some relevance to nanostructured Fe-Co alloys, in that confinement (surface plus finite size) effects may stabilize some of the observed phases. We have already seen that strain effects are important to increase the bcc stability limit down to 0.11 in Fe concentration[9] and that bcc-based nanocrystalline Fe-Co alloys can be produced on the large scale.[91] We believe that our results can be useful in producing and characterizing off-stoichiometry Fe-Co nanoscale alloys.

V. CONCLUDING REMARKS

On the basis of first-principles total-energy calculations of Fe-Co ordered alloys we found a set of new ground states additional to the well-known B2 ordered phase. The magnetic and mechanical properties of these ordered alloys were also calculated. Using the cluster expansion method, the physical quantities of interest were cast into a simple Hamiltonian that allowed for extensive sampling of the configurational space. In particular, for the enthalpy of formation we performed a combinatorial search of 1.5×10^{10} bcc-based configurations that led us to the discovery of the dense sequence of ground states.

The dependence of the magnetic moment, the atomic volume, and the bulk modulus with concentration was also examined rendering a picture where the average magnetic moment is rather insensitive to the configurational details but depends on the atomic concentration and volume. Both the

atomic volume and the magnetic moment resemble those of invar alloys.

Our systematic calculations revealed that Fe_3Co alloys are stable in the $L6_0$ structure (Ti_3Cu-type) thus confirming the early experimental claims on the existence of such superlattices. We do not find, however, unstrained bcc-based $FeCo_3$ superstructures. We argued, on the basis of the experimental evidence and our own calculations, that strain effects might be responsible for stabilizing $FeCo_3$ epitaxial alloys. Certainly, confinement effects may stabilize some of the reported new ordered phases, as the recently reported air-stable Fe-Co nanocrystal superlattices.

We consider that the use of high-throughput *ab initio*-based approaches for bulk materials, as the ones described in this paper, can provide insights into nanoscale alloys. By sampling sizable portions of the configurational phase space, one can identify the neighboring phases that can be reached either by confining the size of the system or by imposing some external fields. Certainly, more work is needed, and we hope this paper motivates both experimental and theoretical investigations along these lines.

ACKNOWLEDGMENTS

Computer resources from the Texas Advanced Supercomputing Center of the University of Texas at Austin are gratefully acknowledged.

APPENDIX: CRYSTAL STRUCTURES

This section aims to provide additional crystallographic information on the structures used for the first-principles calculations of ordered Fe-Co alloys. Commonly found structures, e.g., $D0_3$, as well as superlattices, will not be listed. However, special emphasis has been set on the predicted new ground-state structures, for which the dimensions of the unit cell (in Å) has been given along with the fractional atomic coordinates. In all cases, space group and space group number have been assigned according to Refs. 92 and 93.

1. V_5Zn_4

Prototype structure: V_4Zn_5, Pearson symbol: $tI18$, space group: $I4/mmm$, space group number: 139.

Primitive cell (Cartesian coordinates): $\boldsymbol{a}_1=(-1.5,1.5,0.5)$, $\boldsymbol{a}_2=(1.5,-1.5,0.5)$, $\boldsymbol{a}_3=(1.5,1.5,-0.5)$.

Atomic coordinates (Cartesian coordinates): $A_1=(0.0,0.0,0.0)$, $A_2=(1.0,1.0,0.0)$, $A_3=(1.0,2.0,0.0)$, $A_4=(2.0,1.0,0.0)$, $A_5=(2.0,2.0,0.0)$, $B_1=(0.0,1.0,0.0)$, $B_2=(0.0,2.0,0.0)$, $B_3=(1.0,0.0,0.0)$, $B_4=(2.0,0.0,0.0)$.

2. Cu_4Ti_3

Prototype structure: Cu_4Ti_3, Pearson symbol: $tI14$, space group: $I4/mmm$, space group number: 139.

Primitive cell (Cartesian coordinates): $\boldsymbol{a}_1=(-0.5,0.5,3.5)$, $\boldsymbol{a}_2=(0.5,-0.5,3.5)$, $\boldsymbol{a}_3=(0.5,0.5,-3.5)$.

Atomic coordinates (Cartesian coordinates): $A_1=(0.5,0.5,0.5)$, $A_2=(0.0,0.0,1.0)$, $A_3=(0.5,0.5,2.5)$, $A_4=(0.0,0.0,3.0)$, $B_1=(0.0,0.0,0.0)$, $B_2=(0.5,0.5,1.5)$, $B_3=(0.0,0.0,2.0)$.

3. Al_3Os_2

Prototype structure: Al_3Os_2, Pearson symbol: $tI10$, space group: $I4/mmm$, space group number: 139.

Primitive cell (Cartesian coordinates): $\boldsymbol{a}_1=(-0.5,0.5,2.5)$, $\boldsymbol{a}_2=(0.5,-0.5,2.5)$, $\boldsymbol{a}_3=(0.5,0.5,-2.5)$.

Atomic coordinates (Cartesian coordinates): $A_1=(0.0,0.0,0.0)$, $A_2=(0.0,0.0,1.0)$, $A_3=(0.5,0.5,1.5)$, $B_1=(0.5,0.5,0.5)$, $B_2=(0.0,0.0,2.0)$.

4. Pd_5Ti_3

Prototype structure: Pd_5Ti_3, Pearson symbol: $tP8$, space group: $P4/mmm$, space group number: 123.

Primitive cell (Cartesian coordinates): $\boldsymbol{a}_1=(1.0,0.0,0.0)$, $\boldsymbol{a}_2=(0.0,1.0,0.0)$, $\boldsymbol{a}_3=(0.0,0.0,4.0)$.

Atomic coordinates (Cartesian coordinates): $A_1=(0.0,0.0,0.0)$, $A_2=(0.0,0.0,1.0)$, $A_3=(0.5,0.5,1.5)$, $A_4=(0.5,0.5,2.5)$, $A_5=(0.0,0.0,3.0)$, $B_1=(0.5,0.5,0.5)$, $B_2=(0.0,0.0,2.0)$, $B_3=(0.5,0.5,3.5)$.

5. Fe_8Co_4

Pearson symbol: $oP12$, space group: $Pmma$, space group number: 51.

Primitive cell (Cartesian coordinates): $\boldsymbol{a}_1=(1.0,0.0,0.0)$, $\boldsymbol{a}_2=(0.0,2.0,0.0)$, $\boldsymbol{a}_3=(0.0,0.0,3.0)$.

Atomic coordinates (Cartesian coordinates): $A_1=(0.0,0.0,0.0)$, $A_2=(0.0,0.0,1.0)$, $A_3=(0.5,0.5,1.5)$, $A_4=(0.0,0.0,2.0)$, $A_5=(0.0,1.0,0.0)$, $A_6=(0.5,1.5,0.5)$, $A_7=(0.0,1.0,1.0)$, $A_8=(0.0,1.0,2.0)$, $B_1=(0.5,0.5,0.5)$, $B_2=(0.5,0.5,2.5)$, $B_3=(0.5,1.5,1.5)$, $B_4=(0.5,1.5,2.5)$.

6. GS:FeCo-B2

Prototype structure: CsCl, Pearson symbol: $cP2$, space group: $Pm\bar{3}m$, space group number: 221.

Unit cell parameters: $a=b=c=2.868$ Å, primitive cell: $\boldsymbol{a}_1=(a,0.0,0.0)$, $\boldsymbol{a}_2=(0.0,b,0.0)$, $\boldsymbol{a}_3=(0.0,0.0,c)$.

Fractional atomic coordinates: $Fe_1=(0.0,0.0,0.0)$, $Co_1=(0.5,0.5,0.5)$.

7. GS:Fe_9Co_7

Pearson symbol: $cP16$, space group: $Pm\bar{3}m$, space group number: 221.

Unit cell parameters: $a=b=c=5.739$ Å, primitive cell: $\boldsymbol{a}_1=(a,0.0,0.0)$, $\boldsymbol{a}_2=(0.0,b,0.0)$, $\boldsymbol{a}_3=(0.0,0.0,c)$.

Fractional atomic coordinates: $Fe_1=(-0.25,-0.25,0.25)$, $Fe_2=(-0.25,-0.25,0.75)$, $Fe_3=(-0.25,-0.75,0.25)$, $Fe_4=(-0.25,-0.75,0.75)$, $Fe_5=(-0.75,-0.25,0.25)$, $Fe_6=(-0.75,-0.25,0.75)$, $Fe_7=(-0.75,-0.75,0.25)$, $Fe_8=(-0.50,-0.50,0.50)$, $Fe_9=(-0.75,-0.75,0.75)$, $Co_1=(0.00,0.00,0.00)$, $Co_2=(0.00,0.00,0.50)$, $Co_3=(0.00,$

−0.50,0.00), Co_4=(0.00,−0.50,0.50), Co_5=(−0.50,0.00, 0.00), Co_6=(−0.50,0.00,0.50), Co_7=(−0.50,−0.50,0.00).

8. GS: Fe_5Co_3

Pearson symbol: *cI*8, space group: $Im\bar{3}m$, space group number: 229.

Unit cell parameters: $a=b=c=5.741$ Å, primitive cell: $\boldsymbol{a}_1=\frac{1}{2}(a,b,-c)$, $\boldsymbol{a}_2=\frac{1}{2}(a,-b,c)$, $\boldsymbol{a}_3=\frac{1}{2}(-a,b,c)$.

Fractional atomic coordinates: Fe_1=(0.00,0.00,0.00), Fe_2=(0.50,0.50,0.00), Fe_3=(0.00,0.50,0.00), Fe_4=(0.50, 0.00,0.50), Fe_5=(0.00,0.50,0.50), Co_1=(0.00,0.00,0.50), Co_2=(0.50,0.50,0.50), Co_3=(0.50,0.00,0.00).

9. GS: $Fe_{11}Co_5$

Pearson symbol: *cP*16, space group: *P*4/*mmm*, space group number: 123.

Unit cell parameters: $a=b=c=5.740$ Å, primitive cell: $\boldsymbol{a}_1=(a,0.0,0.0)$, $\boldsymbol{a}_2=(0.0,b,0.0)$, $\boldsymbol{a}_3=(0.0,0.0,c)$.

Fractional atomic coordinates: Fe_1=(−0.25,−0.25,0.25), Fe_2=(0.00,0.00,0.50), Fe_3=(−0.25,−0.25,0.75), Fe_4 =(−0.25,−0.75,0.25), Fe_5=(−0.25,−0.75,0.75), Fe_6 =(−0.75,−0.25,0.25), Fe_7=(−0.75,−0.25,0.75), Fe_8 =(−0.50,−0.50,0.00), Fe_9=(−0.75,−0.75,0.25), Fe_{10} =(−0.50,−0.50,0.50), Fe_{11}=(−0.75,−0.75,0.75), Co_1 =(0.00,0.00,0.00), Co_2=(0.00,−0.50,0.00), Co_3=(0.00, −0.50,0.50), Co_4=(−0.50,0.00,0.00), Co_5=(−0.50,0.00, 0.50).

10. GS: Fe_3Co-$L6_0$

Prototype structure: Ti_3Cu, Pearson symbol: *tP*4, space group: *P*4/*mmm*, space group number: 123.

Unit cell parameters: $a=b=4.067$ Å, $c=2.866$ Å, primitive cell: $\boldsymbol{a}_1=(a,0.0,0.0)$, $\boldsymbol{a}_2=(0.0,b,0.0)$, $\boldsymbol{a}_3=(0.0,0.0,c)$.

Fractional atomic coordinates: Fe_1=(−0.50,−0.50,0.00), Fe_2=(0.00,−0.50,−0.50), Fe_3=(−0.50,0.00,−0.50), Co_1 =(0.00,0.00,0.00).

11. GS: $Fe_{13}Co_3$

Pearson symbol: *cP*16, space group: *P*4/*mmm*, space group number: 123.

Unit cell parameters: $a=b=c=5.750$ Å, primitive cell: $\boldsymbol{a}_1=(a,0.0,0.0)$, $\boldsymbol{a}_2=(0.0,b,0.0)$, $\boldsymbol{a}_3=(0.0,0.0,c)$.

Fractional atomic coordinates: Fe_1=(0.00,0.50,0.00), Fe_2=(−0.25,0.25,0.25), Fe_3=(0.00,0.50,0.50), Fe_4 =(−0.25,0.25,0.75), Fe_5=(−0.25,−0.25,0.25), Fe_6 =(−0.25,−0.25,0.75), Fe_7=(−0.75,0.25,0.25), Fe_8 =(−0.50,0.50,0.50), Fe_9=(−0.75,0.25,0.75), Fe_{10} =(−0.50,0.00,0.00), Fe_{11}=(−0.75,−0.25,0.25), Fe_{12} =(−0.50,0.00,0.50), Fe_{13}=(−0.75,−0.25,0.75), Co_1 =(0.00,0.00,0.00), Co_2=(0.00,0.00,0.50), Co_3=(−0.50, 0.50,0.00).

12. GS: Fe_7Co

Pearson symbol: *cI*8, space group: $Im\bar{3}m$, space group number: 229.

Unit cell parameters: $a=b=c=5.748$ Å, primitive cell: $\boldsymbol{a}_1=\frac{1}{2}(a,b,-c)$, $\boldsymbol{a}_2=\frac{1}{2}(a,-b,c)$, $\boldsymbol{a}_3=\frac{1}{2}(-a,b,c)$.

Fractional atomic coordinates: Fe_1=(0.00,0.00,0.00), Fe_2=(0.50,0.50,0.00), Fe_3=(0.00,0.50,0.00), Fe_4=(0.50, 0.00,0.50), Fe_5=(0.00,0.00,0.50), Fe_6=(0.50,0.50,0.50), Fe_7=(0.50,0.00,0.00), Co_1=(0.00,0.50,0.50).

13. GS: $Fe_{15}Co$

Pearson symbol: *cP*16, space group: $Pm\bar{3}m$, space group number: 221.

Unit cell parameters: $a=b=c=5.746$ Å, primitive cell: $\boldsymbol{a}_1=(a,0.0,0.0)$, $\boldsymbol{a}_2=(0.0,b,0.0)$, $\boldsymbol{a}_3=(0.0,0.0,c)$.

Fractional atomic coordinates: Fe_1=(0.25,0.75,−0.25), Fe_2=(0.00,0.50,0.00), Fe_3=(0.25,0.75,0.25), Fe_4=(0.00, 0.50,0.50), Fe_5=(0.25,0.25,−0.25), Fe_6=(0.25,0.25,0.25), Fe_7=(0.00,0.00,0.50), Fe_8=(−0.25,0.75,−0.25), Fe_9 =(−0.50,0.50,0.00), Fe_{10}=(−0.25,0.75,0.25), Fe_{11} =(−0.50,0.50,0.50), Fe_{12}=(−0.25,0.25,−0.25), Fe_{13} =(−0.50,0.00,0.00), Fe_{14}=(−0.25,0.25,0.25), Fe_{15} =(−0.50,0.00,0.50), Co_1=(0.00,0.00,0.00).

[1] R. S. Sundar and S. C. Deevi, Int. Mater. Rev. **50**, 157 (2005); T. Sourmail, Prog. Mater. Sci. **50**, 816 (2005).

[2] R. E. Quigley, *Proceedings of the IEEE Applied Power Electronics Conference*, 1993, p. 906.

[3] Landolt-Börnstein, *Numerical Data and Functional Relationships in Science and Technology, New Series*, edited by K.-H. Hellwege (Springer, New York, 1979).

[4] T. Nishizawa and K. Ishida, in *Phase Diagrams of Binary Iron Alloys*, edited by T. B. Massalski (Metals Park, OH, 1990), Vol. 2.

[5] H. Masumoto, H. Saito, and M. Shinozaki, Sci. Rep. Res. Inst. Tohoku Univ. A **6**, 523 (1954).

[6] L. M. Viting, Zh. Neorg. Khim. **2**, 375 (1957).

[7] A. A. Goldenberg and Y. P. Selissky, Fiz. Met. Metalloved. **15**, 717 (1963).

[8] H. Asano, Y. Bando, N. Nakanishi, and S. Kachi, Trans. Jpn. Inst. Met. **8**, 180 (1967).

[9] M. Wojcik, J. P. Jay, P. Panissod, E. Jedryka, J. Dekoster, and G. Langouche, Z. Phys. B: Condens. Matter **103**, 5 (1997).

[10] R. Drautz, A. Díaz-Ortiz, M. Fähnle, and H. Dosch, Phys. Rev. Lett. **93**, 067202 (2004).

[11] J. M. Sanchez, F. Ducastelle, and D. Gratias, Physica A **128A**, 334 (1984).

[12] J. M. Sanchez, Phys. Rev. B **48**, 14013 (1993).

[13] K. Schwarz and D. R. Salahub, Phys. Rev. B **25**, 3427 (1982).

[14] J. Kaspar and D. R. Salahub, J. Phys. F: Met. Phys. **13**, 311 (1983).

[15] K. Schwarz, P. Mohn, P. Blaha, and J. Kübler, J. Phys. F: Met.

Phys. **14**, 2659 (1984).
[16] R. J. Hawkins and J. M. Sanchez, J. Phys. F: Met. Phys. **18**, 767 (1988).
[17] A. Y. Liu and D. J. Singh, Phys. Rev. B **46**, 11145 (1992).
[18] S. L. Qiu, P. M. Marcus, and V. L. Moruzzi, J. Appl. Phys. **85**, 4839 (1999).
[19] R. H. Victora and L. M. Falicov, Phys. Rev. B **30**, 259 (1984).
[20] P. Söderlind, O. Eriksson, B. Johansson, R. C. Albers, and A. M. Boring, Phys. Rev. B **45**, 12911 (1992).
[21] R. Richter and H. Eschrig, J. Phys. F: Met. Phys. **18**, 1813 (1988).
[22] I. Turek, J. Kudrnovský, V. Drchal, and P. Weinberger, Phys. Rev. B **49**, 3352 (1994).
[23] I. A. Abrikosov, P. James, O. Eriksson, P. Söderlind, A. V. Ruban, H. L. Skriver, and B. Johansson, Phys. Rev. B **54**, 3380 (1996).
[24] P. James, O. Eriksson, B. Johansson, and I. A. Abrikosov, Phys. Rev. B **59**, 419 (1999).
[25] J. M. MacLaren, T. C. Schulthess, W. H. Butler, R. Sutton, and M. McHenry, J. Appl. Phys. **85**, 4833 (1999).
[26] M. Neumayer and M. Fähnle, Phys. Rev. B **64**, 132102 (2001).
[27] R. Drautz and A. Díaz-Ortiz (unpublished).
[28] S. Curtarolo, D. Morgan, K. Persson, J. Rodgers, and G. Ceder, Phys. Rev. Lett. **91**, 135503 (2003).
[29] D. de Fontaine, Solid State Phys. **47**, 33 (1994).
[30] A. Zunger, in *Statics and Dynamics of Alloy Phase Transformations*, edited by P. E. A. Turchi and A. Gonis (Plenum, New York, 1994), p. 361.
[31] A. van de Walle and G. Ceder, J. Phase Equilib. **23**, 348 (2002).
[32] N. A. Zarkevich and D. D. Johnson, Phys. Rev. Lett. **92**, 255702 (2004).
[33] M. H. F. Sluiter and Y. Kawazoe, Phys. Rev. B **71**, 212201 (2005).
[34] J. W. D. Connolly and A. R. Williams, Phys. Rev. B **27**, 5169 (1983).
[35] Clearly, an arbitrary choice of the structure weights f_i can lead to unphysical expansions. We suggest $f_i=1$ unless an important property (e.g., the ground-state line) of the system cannot be described otherwise.
[36] G. L. W. Hart, V. Blum, M. J. Walorski, and A. Zunger, Nat. Mater. **4**, 391 (2005); V. Blum, G. L. W. Hart, M. J. Walorski, and A. Zunger, Phys. Rev. B **72**, 165113 (2005).
[37] B. Meyer, C. Elsässer, F. Lechermann, and M. Fähnle, "FORTRAN90 Program for Mixed-Basis Pseudopotential Calculations," Max-Planck-Institut für Metallforschung, Stuttgart (unpublished).
[38] D. Vanderbilt, Phys. Rev. B **32**, 8412 (1985).
[39] S. G. Louie, S. Froyen, and M. L. Cohen, Phys. Rev. B **26**, 1738 (1982).
[40] J. P. Perdew, K. Burke, and M. Ernzerhof, Phys. Rev. Lett. **77**, 3865 (1996); **78**, 1396 (1997).
[41] J. Moreno and J. M. Soler, Phys. Rev. B **45**, 13891 (1992).
[42] J. P. Perdew and Y. Wang, Phys. Rev. B **33**, 8800 (1986).
[43] J. P. Perdew and Y. Wang, Phys. Rev. B **45**, 13244 (1992).
[44] G. Kresse and J. Hafner, Phys. Rev. B **47**, 558 (1993); **49**, 14251 (1994); Comput. Mater. Sci. **6**, 15 (1996); G. Kresse and J. Furthmüller, Phys. Rev. B **54**, 11169 (1996).
[45] F. Lechermann, M. Fähnle, and J. M. Sanchez, Intermetallics **13**, 1096 (2005).
[46] J. Zhu, X. W. Wang, and S. G. Louie, Phys. Rev. B **45**, 8887 (1992).
[47] C. Elsässer, J. Zhu, S. G. Louie, M. Fähnle, and C. T. Chan, J. Phys.: Condens. Matter **10**, 5081 (1998).
[48] D. J. Singh, W. E. Pickett, and H. Krakauer, Phys. Rev. B **43**, 11628 (1991).
[49] L. Stixrude, R. E. Cohen, and D. J. Singh, Phys. Rev. B **50**, 6442 (1994).
[50] H. C. Herper, E. Hoffmann, and P. Entel, Phys. Rev. B **60**, 3839 (1999).
[51] C. Amador, W. R. L. Lambrecht, and B. Segall, Phys. Rev. B **46**, 1870 (1992).
[52] J.-H. Cho and M. Scheffler, Phys. Rev. B **53**, 10685 (1996).
[53] E. G. Moroni, G. Kresse, J. Hafner, and J. Furthmüller, Phys. Rev. B **56**, 15629 (1997).
[54] G. Kresse and D. Joubert, Phys. Rev. B **59**, 1758 (1999).
[55] S. Fox and H. J. F. Jansen, Phys. Rev. B **60**, 4397 (1999).
[56] D. J. Singh, Phys. Rev. B **45**, 2258 (1992); A. Y. Liu and D. J. Singh, J. Appl. Phys. **73**, 6189 (1993); Phys. Rev. B **47**, 8515 (1993).
[57] M. Komelj and M. Fähnle, Phys. Rev. B **73**, 012404 (2006).
[58] B. I. Min, T. Oguchi, and A. J. Freeman, Phys. Rev. B **33**, 7852 (1986).
[59] V. L. Moruzzi, P. M. Marcus, K. Schwarz, and P. Mohn, Phys. Rev. B **34**, 1784 (1986).
[60] L. T. Kong, R. F. Zhang, Z. C. Li, and B. X. Liu, Phys. Rev. B **68**, 134446 (2003).
[61] G. A. Prinz, Phys. Rev. Lett. **54**, 1051 (1985); Y. U. Idzerda, W. T. Elam, B. T. Jonker, and G. A. Prinz, Phys. Rev. Lett. **62**, 2480 (1989); S. Subramanian, R. Sooryakumar, G. A. Prinz, B. T. Jonker, and Y. U. Idzerda, Phys. Rev. B **49**, 17319 (1994).
[62] D. Bagayoko, A. Ziegler, and J. Callaway, Phys. Rev. B **27**, 7046 (1983).
[63] G. A. Prinz, J. Magn. Magn. Mater. **100**, 469 (1991).
[64] D. J. Singh, J. Appl. Phys. **71**, 3431 (1992).
[65] P. Vinet, J. R. Smith, J. Ferrante, and J. H. Rose, Phys. Rev. B **35**, 1945 (1987); P. Vinet, J. Ferrante, J. R. Smith, and J. H. Rose, J. Phys. C **19**, L467 (1986); J. H. Rose, J. Ferrante, and J. R. Smith, Phys. Rev. Lett. **47**, 675 (1981); J. R. Smith, J. Ferrante, and J. H. Rose, Phys. Rev. B **25**, 1419 (1982); J. H. Rose, J. R. Smith, F. Guinea, and J. Ferrante, Phys. Rev. B **29**, 2963 (1984).
[66] D. F. Shanno and K. H. Phua, ACM Trans. Math. Softw. **2**, 87 (1976).
[67] In the fully disordered state, the average of product of occupation variables can be replaced by the product of the average of the occupation variables. This translates in that the multisite correlation functions Φ_α appearing in Eq. (1) can be written as $\Phi_\alpha = (2x-1)^{|\alpha|}$ with $|\alpha|$ the number of sites in cluster α.
[68] M. Sanati, L. G. Wang, and A. Zunger, Phys. Rev. Lett. **90**, 045502 (2003); J. S. Anderson, J. Chem. Soc. Dalton Trans. **10**, 1107 (1973); C. Kittel, Solid State Commun. **25**, 519 (1978).
[69] V. Blum and A. Zunger, Phys. Rev. B **72**, 020104(R) (2005).
[70] J. W. Rodgers and W. R. Maddocks, Second Report of the Alloy Steels Research Committee, No. 24, 1939, p. 167, as cited by Ellis and Greiner in Ref. 71.
[71] W. C. Ellis and E. S. Greiner, Trans. Am. Soc. Met. **29**, 415 (1941).
[72] F. Lechermann, F. Welsch, C. Elsässer, C. Ederer, M. Fähnle, J. M. Sanchez, and B. Meyer, Phys. Rev. B **65**, 132104 (2002).
[73] D. I. Bardos, J. Appl. Phys. **40**, 1371 (1969).
[74] R. A. Reck and D. L. Fry, Phys. Rev. **184**, 492 (1969).
[75] O. K. Andersen, O. Jepsen, and G. Krier, in *Lectures on Methods*

of Electronic Structure Calculations, edited by V. Kumar, O. Andersen, and A. Mookerjee (World Scientific, Singapore, 1994).

[76] L. V. Pourovskii, A. V. Ruban, L. Vitos, H. Ebert, B. Johansson, and I. A. Abrikosov, Phys. Rev. B **71**, 094415 (2005).

[77] E. Engel and S. H. Vosko, Phys. Rev. A **47**, 2800 (1993); S. Kümmel and J. P. Perdew, Phys. Rev. B **68**, 035103 (2003).

[78] E. Di Fabrizio, G. Mazzone, C. Petrillo, and F. Sacchetti, Phys. Rev. B **40**, 9502 (1989).

[79] J. P. Perdew, A. Ruzsinszky, J. Tao, V. N. Staroverov, G. E. Scuseria, and G. I. Csonka, J. Chem. Phys. **123**, 062201 (2005).

[80] J. Tao, J. P. Perdew, V. N. Staroverov, and G. E. Scuseria, Phys. Rev. Lett. **91**, 146401 (2003).

[81] A. R. Williams, V. L. Moruzzi, A. P. Malozemoff, and K. Tekura, IEEE Trans. Magn. **MAG-19**, 1983 (1983).

[82] Y. Nakamura, IEEE Trans. Magn. **MAG-12**, 278 (1976).

[83] L. Pauling, Phys. Rev. **54**, 899 (1938).

[84] J. Kübler, *Theory of Itinerant Electron Magnetism* (Clarendon, Oxford, 2000).

[85] J. Ph. Jay, M. Wojcik, and P. Panissod, Z. Phys. B: Condens. Matter **101**, 471 (1996).

[86] L. M. Falicov, D. T. Pierce, S. D. Bader, R. Gronsky, K. B. Hathaway, H. J. Hopster, D. N. Lambeth, S. S. P. Parkin, G. Prinz, M. Salamon, I. K. Schuller, and R. H. Victora, J. Mater. Res. **5**, 1299 (1990); H. Dosch, *Critical Phenomena at Surface and Interfaces* (Springer, Berlin, 1992).

[87] D. Young, *Phase Diagrams of the Elements* (University of California Press, Berkeley, 1991).

[88] A. Díaz-Ortiz, J. M. Sanchez, and J. L. Morán-López, Phys. Rev. Lett. **81**, 1146 (1998); Phys. Rev. B **62**, 1148 (2000).

[89] T. Schülli, J. Tenkler, I. Mönch, D. Le Bolloch, and H. Dosch, Europhys. Lett. **58**, 737 (2002).

[90] C. Suryanarayana, in *Intermetallic Compounds*, edited by J. H. Westbrook and R. L. Fleischer (Wiley, New York, 2002), Vol. 3.

[91] C. Desvaux, C. Amiens, P. Fejes, P. Renaud, M. Respaud, P. Lecante, E. Snoeck, and B. Chaudret, Nat. Mater. **4**, 750 (2005).

[92] R. Hund, KPLOT, University of Bonn, Germany, 1979; A. Hannemann, R. Hundt, J. C. Schön, and M. Jensen, J. Appl. Crystallogr. **31**, 9222 (1998); R. Hund, J. C. Schön, A. Hannemann, and M. Jensen, *ibid.* **32**, 413 (1999).

[93] *International Tables for Crystallography*, 2nd. revised edition (Reidel, Dordrecht, 1987).